International Journal of Nanomedicine

Dovepress
open access to scientific and medical research

Open Access Full Text Article

ORIGINAL RESEARCH

Fe_3O_4@Au composite magnetic nanoparticles modified with cetuximab for targeted magneto-photothermal therapy of glioma cells

This article was published in the following Dove Press journal:
International Journal of Nanomedicine

Qianling Lu,[1,*] Xinyu Dai,[1,*] Peng Zhang,[1,*] Xiao Tan,[2] Yuejiao Zhong,[3] Cheng Yao,[4] Mei Song,[4] Guili Song,[4] Zhenghai Zhang,[4] Gang Peng,[5] Zhirui Guo,[6] Yaoqi Ge,[7] Kangzhen Zhang,[7] Yuntao Li[7]

[1]Department of Neurology, Second Affiliated Hospital of Nanjing Medical University, Nanjing, China; [2]Department of Emergency, Second Affiliated Hospital of Nanjing Medical University, Nanjing, China; [3]Department of Oncology, The Affiliated Cancer Hospital of Nanjing Medical University, Nanjing, China; [4]Office of Academic Research, Kizilsu Kirghiz Autonomous Prefecture People's Hospital, Atush, China; [5]Department of Neurosurgery, Second Affiliated Hospital of Nanjing Medical University, Nanjing, China; [6]Department of Geratology, Second Affiliated Hospital of Nanjing Medical University, Nanjing, China; [7]Department of General Practice, Second Affiliated Hospital of Nanjing Medical University, Nanjing, China

*These authors contributed equally to this work

Background: Thermoresponsive nanoparticles have become an attractive candidate for designing combined multimodal therapy strategies because of the onset of hyperthermia and their advantages in synergistic cancer treatment. In this paper, novel cetuximab (C225)-encapsulated core-shell Fe_3O_4@Au magnetic nanoparticles (Fe_3O_4@Au-C225 composite-targeted MNPs) were created and applied as a therapeutic nanocarrier to conduct targeted magneto-photothermal therapy against glioma cells.

Methods: The core-shell Fe_3O_4@Au magnetic nanoparticles (MNPs) were prepared, and then C225 was further absorbed to synthesize Fe_3O_4@Au-C225 composite-targeted MNPs. Their morphology, mean particle size, zeta potential, optical property, magnetic property and thermal dynamic profiles were characterized. After that, the glioma-destructive effect of magnetic fluid hyperthermia (MFH) combined with near-infrared (NIR) hyperthermia mediated by Fe_3O_4@Au-C225 composite-targeted MNPs was evaluated through in vitro and in vivo experiments.

Results: The inhibitory and apoptotic rates of Fe_3O_4@Au-C225 composite-targeted MNPs-mediated combined hyperthermia (MFH+NIR) group were significantly higher than other groups in vitro and the marked upregulation of caspase-3, caspase-8, and caspase-9 expression indicated excellent antitumor effect by inducing intrinsic apoptosis. Furthermore, Fe_3O_4@Au-C225 composite-targeted MNPs-mediated combined hyperthermia (MFH+NIR) group exhibited significant tumor growth suppression compared with other groups in vivo.

Conclusion: Our studies illustrated that Fe_3O_4@Au-C225 composite-targeted MNPs have great potential as a promising nanoplatform for human glioma therapy and could be of great value in medical use in the future.

Keywords: Fe_3O_4@Au-C225 composite-targeted magnetic nanoparticles, U251 cells, human glioma therapy, magnetic fluid hyperthermia, near-infrared hyperthermia

Introduction

Gliomas are primary brain tumors arising from the supporting cells of the brain or spinal cord. Accounting for >30% of all primary brain and central nervous system (CNS) malignant tumors, gliomas are the most common tumors of the CNS. They involve almost 80% of primary malignant type of brain tumors and are responsible for a higher rate of mortality than other forms.[1] Overall incidence rate for primary malignant brain and CNS tumors is estimated to be 7.27/100,000 per year for all age groups.[2] The International Agency for Research on Cancer data estimate 256,213 worldwide cases of brain and CNS tumors, which is 1.8% of all estimated cancers, and 189,394 deaths, which is 2.3% of all cancer-related deaths.[3] An estimated 16,700 deaths were attributed to high-grade gliomas in the brain and CNS in the USA in 2017.[4] These aggressive brain tumors

Correspondence: Yuntao Li
Department of General Practice, Second Affiliated Hospital of Nanjing Medical University, No 121 Jiangjiayuan Road, Nanjing 210011, China
Tel +86 25 5850 9989
Fax +86 25 5850 9989
Email liyuntao78@163.com

Yuejiao Zhong
Department of Oncology, The Affiliated Cancer Hospital of Nanjing Medical University, Baiziting 42, Nanjing 210009, China
Email zhongyuejiao@163.com

submit your manuscript | www.dovepress.com
Dovepress
http://dx.doi.org/10.2147/IJN.S157935

grow invasively and cause discernible neurologic symptoms within months with an extremely poor prognosis. Even treated with aggressive open surgery combined with adjuvant chemo/radiotherapy, the median survival time is still <15 months,[5–8] and current treatment paradigms appear to have reached their maximum benefit. Therefore, for decades, considerable efforts have been devoted to developing more effective antitumor agents and better strategies for targeting human glioma.[9,10]

Recently, nanostructures with combined diagnostic and therapeutic functions represent a potential application for tumor therapy.[11–14] Many inorganic nanoparticles with various compositions, physical features, and functionalities have been widely synthesized and used as drug vehicles, for instance, polymer Prussian blue, zeolitic imidazolate framework, alginate, and calcium phosphate.[15–18] Likewise, metal nanoparticles and their oxides with special shapes (sphere, tadpole, and pearl chain) have been successfully generated. Magnetic nanoparticles (MNPs), such as iron oxide, have been widely studied because of their combination of properties such as superparamagnetism, biocompatibility, and ease of synthesis. The most common form of iron oxide used is magnetite (Fe_3O_4) with a tendency to oxidize, which alters its magnetic properties.[19] That is why iron oxide nanoparticles are generally coated with a biocompatible layer such as polymers, silica, or gold (Au).[20–27]

In particular, core-shell-structured Fe_3O_4@Au composite MNPs have been the focus of study owing to their intriguing bifunctional properties.[28,29] As a form of multifunctional magnetoplasmonic nanomaterials, the nanoparticles combining Au and magnetic materials inherit from the two components excellent surface chemistry, special optical properties, and superparamagnetic properties, all of which would greatly enhance the potential and broaden the practical applications of such nanomaterials.[30]

Advances in the area of nanotechnology have contributed to the development of magnetic fluid hyperthermia (MFH). In vivo MFH is expected to be one of the best solutions for destroying tumor cells that are deeply seated and localized inside the human body for unlimited tissue penetration and the possibility of multiple hyperthermia cycles. Additionally, high selectivity and heating homogeneity can be expected in the use of MFH. Nevertheless, the practical limitation with MFH is that heating efficiency declines markedly when nanoparticles are taken up by cancer cells, because their endocytosis and aggregation inhibit their Brownian motion. Similarly, the diffusion (thereby local dilution) or enhanced distribution of nanoparticles also decreases nanoparticle heating.[31] The drawbacks of MFH could be overcome by combination with near-infrared (NIR) hyperthermia. With local plasmonic heating caused by NIR laser excitation, its efficiency is not impacted by intracellular confinement.[31] As a form of multifunctional magnetoplasmonic nanomaterials, Fe_3O_4@Au composite MNPs are the designs of choice to implement a magneto-photothermal strategy to optimize nanoparticles' heating efficiency.

We previously reported self-prepared Fe_3O_4@Au composite MNPs, which are intrinsically magnetic, and exhibit high biocompatibility and safety according to the evaluation of toxicity in vivo and in vitro.[32] Moreover, these MNPs have a potential to be used as safe optical and thermal agents, allowing the combination of cancer detection and cancer-specific hyperthermic treatment.[32] The present study is aimed at the functionalization of Fe_3O_4@Au composite MNPs with cetuximab (C225), a monoclonal antibody (McAb) targeting the epidermal growth factor receptor (EGFR) overexpressed in cancer cells. Additionally, the antiglioma effects of MFH combined with NIR hyperthermia mediated by Fe_3O_4@Au-C225 composite-targeted MNPs were also investigated with in vitro and in vivo experiments.

Experimental

Materials

4-(2-Hydroxyethyl)-1-piperazineethanesulfonic acid and trypsin were purchased from AMRESCO. Bovine serum albumin (BSA) was purchased from Sijiqing Hangzhou Bioengineering Company. Dulbecco's Modified Eagle's Medium (DMEM) was purchased from GIBCO BD. MTT, diethylpyrocarbonate, and ethidium bromide were purchased from Sigma. Dimethyl sulfoxide was purchased from Shanghai Ling Feng Chemical Co., Ltd. RNAiso Reagent, AMV reverse transcriptase, deoxyribonucleoside triphosphate (dNTP), Oligo(dT)18, Taq DNA polymerase, 100 bp DNA Marker, RNasin, and RNase free DNase I were purchased from Takara. From Shanghai Shenneng Gaming Biotechnology Co. Ltd. (Whitehouse Station, NJ, USA), 20×TBE, agarose, caspase-3 primer, caspase-8 primer, caspase-9 primer, and β-actin primer were purchased. C225 solution for infusion was purchased from Merck & Co, Germany. All other chemicals were commercially available and of analytical grade.

Cells and animals

U251 cells (human glioma cells) were purchased from Shanghai Cell Research Institute of Chinese Academy of Sciences. Balb/c nu/nu nude mice (5–7 weeks old, male and female, SPF grade) were purchased from Slaccas (Shanghai, China). License number: SCXK (Shanghai) 2002-0010. All of them were raised in Experimental Animal Center of Southeast University, Nanjing, China. All experiments involving

animals were performed in compliance with the guidelines of the Animal Care Committee of the Southeast University (Nanjing, China; Approval ID: SYXK-20140310358). All animals received humane care in compliance with the "Principles of Laboratory Animal Care" formulated by the National Society for Medical Research and the "Guide for the Care and Use of Laboratory Animals" prepared by the Institute of Laboratory Animal Resources and published by the National Institutes of Health (NIH Publication No 86-23, revised 1996).

Preparation of Fe_3O_4@Au-C225 MNPs

Fe_3O_4 MNPs were prepared by chemical co-precipitation method as previously published.[33] Then Fe_3O_4 MNP solution was stirred with sodium citrate (1 mmol/L, 20 mL) for 10 min. The mixture was diluted with deionized water and NH_2OH_3HCl (1 mol/L, 1 mL) was added. After that, $HAuCl_4$ (1%, 10 mL) was incrementally added dropwise with stirring for 1 h. Fe_3O_4@Au MNPs were separated by means of a permanent magnet and stored for further use.[32] Next, C225 was loaded onto Fe_3O_4@Au MNPs via physical adsorption. C225 (5 mg/mL, 20 μL) was added into solution of Fe_3O_4@Au MNPs (0.5 mg Fe/mL, 2.5 mL) whose value of pH was adjusted to 9.0 by HCl (0.1 mol/L), and the mixture was placed in a temperature-controlled shaker at 200 rpm for 2 h at a given temperature of 37°C, followed by BSA (1%, 100 μL) added for reaction for 30 min. At the end of the adsorption, the supernatant and Fe_3O_4@Au-C225 MNPs were separated by means of a permanent magnet, and the obtained precipitate was dissolved in BSA (1%, 1 mL) and stored at 4°C for further use.

Characterization of Fe_3O_4@Au-C225 MNPs

The morphology of Fe_3O_4@Au-C225 MNPs was characterized using transmission electron microscopy (TEM; JEM-1011; JEOL, Tokyo, Japan) and scanning electron microscopy (SEM; JSM-6360LV; JEOL, Tokyo, Japan). The mean particle size and zeta potential were measured using Malvern Instruments (Malvern, UK). The optical properties and magnetic property were measured using 752 Prismatic UV−vis spectroscopy (Shanghai Precision Scientific Instrument Co., China) and vibrating sample magnetometer (PPMS-9; Quantum Design, USA).

Determination of C225 on the surface of Fe_3O_4@Au-C225 MNPs

To confirm whether the C225 was linked to Fe_3O_4@Au-C225 MNPs, the fluorescein isothiocyanate (FITC)-conjugated AffiniPure Goat Anti-Human Immunoglobulin G (IgG) was added to 2 μL of Fe_3O_4@Au-C225 MNPs with 1% BSA and allowed to react for 1 h at 37°C. After separated by means of a permanent magnet, the precipitate was washed three times with PBS, redispersed in 20 μL of PBS, and observed under a confocal laser scanning microscope (Leica TCS SP8 STED 3×; Leica Microsystems, Wetzlar, Germany). Fe_3O_4@Au MNPs were used as control.

Adsorption efficiency measurements

To determine the antibody absorption efficiency, the FITC-conjugated AffiniPure Goat Anti-Human IgG was added to 2 μL of Fe_3O_4@Au-C225 MNPs with 1% BSA and allowed to react for 1 h at 37°C in the dark. After separated by means of a permanent magnet, the precipitate was washed three times with PBS, redispersed in 20 μL of PBS, and observed under a confocal laser scanning microscope (Leica TCS SP8 STED 3×). Fe_3O_4@Au-C225 MNPs that were not incubated with FITC-conjugated AffiniPure Goat Anti-Human IgG were used as control. The image data were processed with ImageJ software 1.8.

The effective Fc binding of C225 toward the surface of the Fe_3O_4@Au MNPs was also investigated by enzyme-linked immunosorbent assay according to the literature procedure.[34] Goat Anti-Human IgG (Fc)-horseradish peroxidase (HRP) was, respectively, added into an aqueous solution of Fe_3O_4@Au-C225 MNPs (100 μL) at dilutions of 1:500, 1:1,000, 1:2,000, 1:4,000, 1:8,000, and 1:16,000, and incubated for 1 h at 37°C. After separated by means of a permanent magnet (60 min, 4°C), supernatant (100 μL) was then collected, and ortho-phenylenediamine substrate solution was added at room temperature protected from light. After 10 min, the reaction was stopped by adding H_2SO_4 (2 mol/L, 50 μL). Part of the dye solution was transferred and the OD was measured at 492 nm with a plate reader. Served as control, treatment of Fe_3O_4@Au-BSA and C225 mixture followed the same procedure described above.

Heating test of the Fe_3O_4@Au-C225 MNPs

The Fe_3O_4@Au-C225 MNPs' magnetothermal and photothermal effects were tested in aqueous suspensions as a function of [Fe] concentrations, ranging from 0.25 to 1.25 mg Fe/mL. The [Fe] concentrations of the samples dispersed in deionized water were analyzed using Leeman Prodigy inductively coupled plasma-optical emission spectroscopy (USA). Three heating protocols were selected: 1) alternating magnetic field (AMF) alone, at an output frequency of 230 kHz and an output current of 30 A; 2) NIR laser alone at 635 nm laser with 0.3 W/cm²; and 3) combined hyperthermia (simultaneous application of both AMF and NIR).

Cell culture

U251 cell line was maintained in DMEM, supplemented with 10% fetal bovine serum in a standard humidified 5% CO_2 and 37°C incubator. The cells were passaged every 2–3 days and harvested on exponential growth stage.

Study of Fe_3O_4@Au-C225 MNPs on human glioma U251 cells in vitro

Observation of U251 cells labeled by Fe_3O_4@Au-C225 MNPs

U251 cells were seeded into four holes of a six-well plate with fresh growth medium and incubated (37°C, 5% CO_2) overnight to bring the cells to confluence (1×10^6 cells). The growth medium was then discarded and replaced with fresh medium containing Fe_3O_4 MNPs, Fe_3O_4@Au MNPs, and Fe_3O_4@Au-C225 MNPs at the same [Fe] concentration and PBS as control. The cells were incubated (37°C, 5% CO_2) for an additional 24 h and observed with an inverted microscope (Nikon, Tokyo, Japan).

MTT assay of antiproliferative effect

U251 cells (4×10^4/mL) were cultured in four 96-well plates (100 µL/well) and incubated in an incubator (37°C, 5% CO_2). After incubation for 24 h, the growth medium containing different reagents (Fe_3O_4 MNPs [0.5 mg Fe/mL], C225 [50 µg/mL], Fe_3O_4@Au MNPs [0.5 mg Fe/mL], Fe_3O_4@Au-C225 MNPs [0.5 mg Fe/mL]) was added into the wells of experimental groups (eight wells/group) and DMEM as negative control. Four plates were exposed to nonhyperthermia or AMF alone or NIR alone or AMF+NIR, respectively. Nonhyperthermia plate was exposed to no heat treatment. AMF plate was placed into AMF (f=230 kHz, I=30 A) for 30 min. NIR plate was treated with NIR laser (λ=635 nm, 0.3 W/cm^2) for 30 min. AMF+NIR plate was possessed with simultaneous application of both AMF and NIR. After incubation for an additional 24 h, the cell viability was measured by a standard MTT method and the cell absorbance was measured at an OD of 492 nm. The cell relative growth rate (RGR) was calculated as (OD of experimental group/OD of blank control group)×100%.

Flow cytometry evaluation of cell apoptosis

U251 cells were seeded in culture flasks (6×10^5 cells/flask) and divided into eight groups as follows: 1) blank; 2) Fe_3O_4@Au MNPs+MFH; 3) Fe_3O_4@Au MNPs+NIR; 4) Fe_3O_4@Au MNPs+MFH+NIR; 5) Fe_3O_4@Au-C225 MNPs; 6) Fe_3O_4@Au-C225 MNPs+MFH; 7) Fe_3O_4@Au-C225 MNPs+NIR; and 8) Fe_3O_4@Au-C225 MNPs+MFH+NIR. Cells were incubated with Fe_3O_4@Au-C225 MNPs (0.5 mg Fe/mL, 5 mL), Fe_3O_4@Au MNPs (0.5 mg Fe/mL, 5 mL), and medium solution (5 mL) in a humidified incubator (37°C, 5% CO_2) for 24 h, respectively. For MFH, cells were placed into AMF (f=230 kHz, I=30 A) for 30 min. For photothermotherapy, cells were treated with NIR laser light (λ=635 nm, 0.3 W/cm^2) for 30 min. For combined hyperthermia, cells were possessed with simultaneous application of both MFH and NIR. After incubation for an additional 48 h, cells were collected, washed twice with PBS, and fixed overnight in 70% ethanol at 4°C. Cells were than washed with PBS and stained with propidium iodide for 30 min at room temperature in the dark. Cell cycle analysis was performed with an FACS Vantage SE flow cytometer (Becton-Dickinson, Franklin Lakes, NJ, USA).

Quantitative real-time polymerase chain reaction (qRT-PCR)

U251 cells were divided and treated according to the protocol described in the study using flow cytometer assay. After treatment, total RNA was extracted from groups of cells using RNAiso Reagent from Takara and dissolved in DEPC-treated water. Reverse transcription was performed with a 20 µL total volume comprising 2 µL of extracted RNA, 1 µL of Takara Oligo dT_{18}, 2 µL of Takara dNTP (10 mM), 0.5 µL of Takara RNasin, 1 µL of Takara AMV, 4 µL of 5× AMV Buffer, and 9.5 µL of DEPC-treated water. The qRT-PCR was performed in a 25 µL total volume comprising 2 µL of 10× PCR buffer, 2 µL of Takara dNTP (2.5 mM), 1 µL of 5′ primer (20 pmol/µL), 1 µL of 3′ primer (20 pmol/µL), 0.5 µL of Takara TaqE (5 U/µL), 2.5 µL of $MgCl_2$ (25 mM), 11 µL of DEPC-treated water, and 5 µL of cDNA on the PTC-100 (MJ Research, Inc., Watertown, MA, USA). The sequences of the specific primers used in the research were as follows: caspase-3 – forward: 5′-AAACAGTATGCCGACAAG-3′ and reverse: 5′-GAGGGAAATACAGTACCAAA-3′; caspase-8 – forward: 5′-AAAGGGAACTTCAGACACC-3′ and reverse: 5′-CAGCAGGCTCTTGTTGAT-3′; caspase-9 – forward: 5′-CGAACTAACAGGCAAGCA-3′ and reverse: 5′-TTCACCTCCACCATGAAAT-3′; β-actin – forward: 5′-CGTCTGGACCTGGCTGGCCGGGACC-3′ and reverse: 5′-CATGAAGCATTTGCGGTGGACGATG-3′. The melting curve and threshold cycle data for each PCR product were determined and analyzed.

Western blotting

U251 cells were divided and treated according to the protocol described in the study using flow cytometry assay. Cells under different treatments were lysed, and the protein concentrations were assessed using Bradford assay. Proteins were separated using sodium dodecyl sulfate-polyacrylamide gel electrophoresis and transferred from gel to polyvinylidene difluoride

membranes. The membranes were blocked with nonfat milk and probed with primary antibodies followed by HRP-conjugated secondary antibodies and the signals were detected.

Study of Fe_3O_4@Au-C225 MNPs on human glioma U251 cells in vivo

Establishment and treatments of a nude mouse xenograft model of human glioma

All the animal experiments were approved by the animal protection and care Committee of Southeast University. Balb/c nu/nu nude mice (Slaccas Shanghai, China) aged 5–7 weeks were used.

U251 cells (2×10^6 cell/site) were implanted subcutaneously into nude mice and allowed to grow for 20–25 days after inoculation. As the tumors grew to approximately a diameter of 0.5 cm, the mice were randomly divided into eight groups with six mice in each group as follows: 1) negative control; 2) Fe_3O_4@Au MNPs+MFH; 3) Fe_3O_4@Au MNPs+NIR; 4) Fe_3O_4@Au MNPs+MFH+NIR; 5) Fe_3O_4@Au-C225 MNPs; 6) Fe_3O_4@Au-C225 MNPs+MFH; 7) Fe_3O_4@Au-C225 MNPs+NIR; and 8) Fe_3O_4@Au-C225 MNPs+MFH+NIR.

Tumor volumes (V, mm^3) were calculated using the formula $V=(a\times b^2)/2$, where a and b refer to the length and width of the tumor, respectively. After that, Fe_3O_4@Au MNPs (0.5 mg Fe/mL) and Fe_3O_4@Au-C225 MNPs (0.5 mg Fe/mL) were peritumorally injected at a dose of one-third of tumor volume, respectively. For MFH, the tumors were exposed to AMF (f=230 kHz, I=30 A) three times for 30 min each and a time interval of 24 h. For photothermotherapy, the tumors were irradiated with NIR laser light (λ=635 nm, 0.3 W/cm^2) three times for 30 min each and a time interval of 24 h. For combined hyperthermia, tumors were possessed with simultaneous application of both MFH and NIR.

Tumor growth evaluation

The mice were killed on day 42 after the initial treatment. The quality and volume of stripped tumors were measured. Tumors and major organs (heart, liver, spleen, kidneys, lungs, and tumor) were surgically removed at the end of the treatment after killing. The tissues were fixed in 4% formaldehyde and embedded in paraffin, sectioned into thick slices, and stained with hematoxylin/eosin. Ultrastructural characteristics of the tumor were observed by TEM.

Statistical analysis

All statistical analyses were performed using SPSS version 19.0 software (SPSS Inc., Chicago, IL, USA). Results were expressed as mean ± SD. Statistically significant differences were assessed via analysis of variance. Statistical significance was set at $P<0.05$.

Results

Preparation and characterization of Fe_3O_4@Au-C225 MNPs

Fe_3O_4@Au MNPs were synthesized as previously reported, and the C225 loading was achieved via physical adsorption.[32] TEM and SEM micrographs (Figure 1) show that prepared Fe_3O_4@Au-C225 MNPs were approximately spherical and uniform with good dispersibility.

The Fe_3O_4@Au-C225 MNPs had an average hydrodynamic diameter of 46 nm with single peak shape and narrow particle size distribution (Figure 2A) compared to Fe_3O_4@Au MNPs (35 nm).[32] The zeta potential of Fe_3O_4@Au-C225 MNPs was positive at 11.1±1.8 mV in the neutral environment of pH 7.4 (Figure 2B), as a result of the presence of the C225 as part of the overall MNP structure. The clusters of Fe_3O_4@Au-C225 MNPs were observed in TEM and SEM. It may be attributable to slightly decreased electrostatic force between the positively charged Fe_3O_4@Au-C225 MNPs according to the decreased zeta potential (11.1±1.8 mV) compared to negatively charged Fe_3O_4@Au MNPs (–23.2±1.8 mV).[32]

Differences in the chemical structure between Fe_3O_4@Au-C225 MNPs and Fe_3O_4@Au MNPs also resulted in

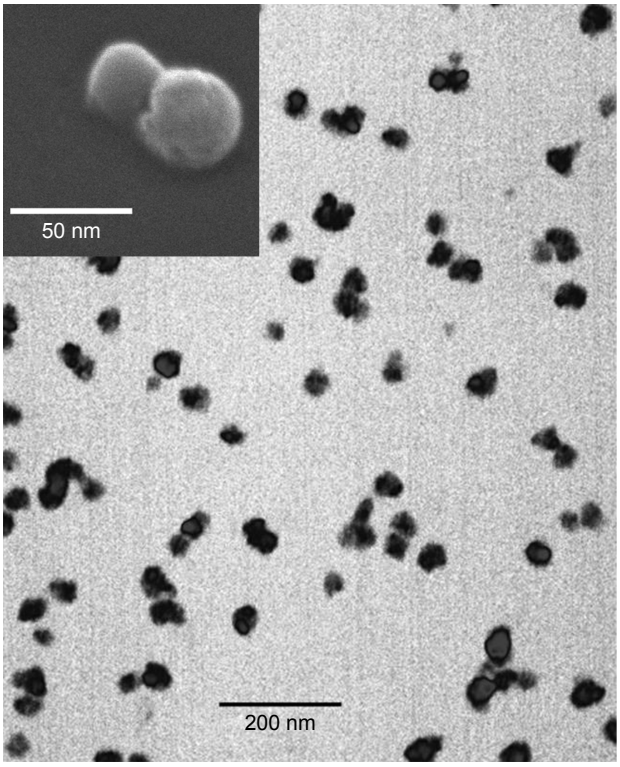

Figure 1 Transmission electron microscopy and scanning electron microscopy (top) of Fe_3O_4@Au-C225 magnetic nanoparticles.
Abbreviation: C225, cetuximab.

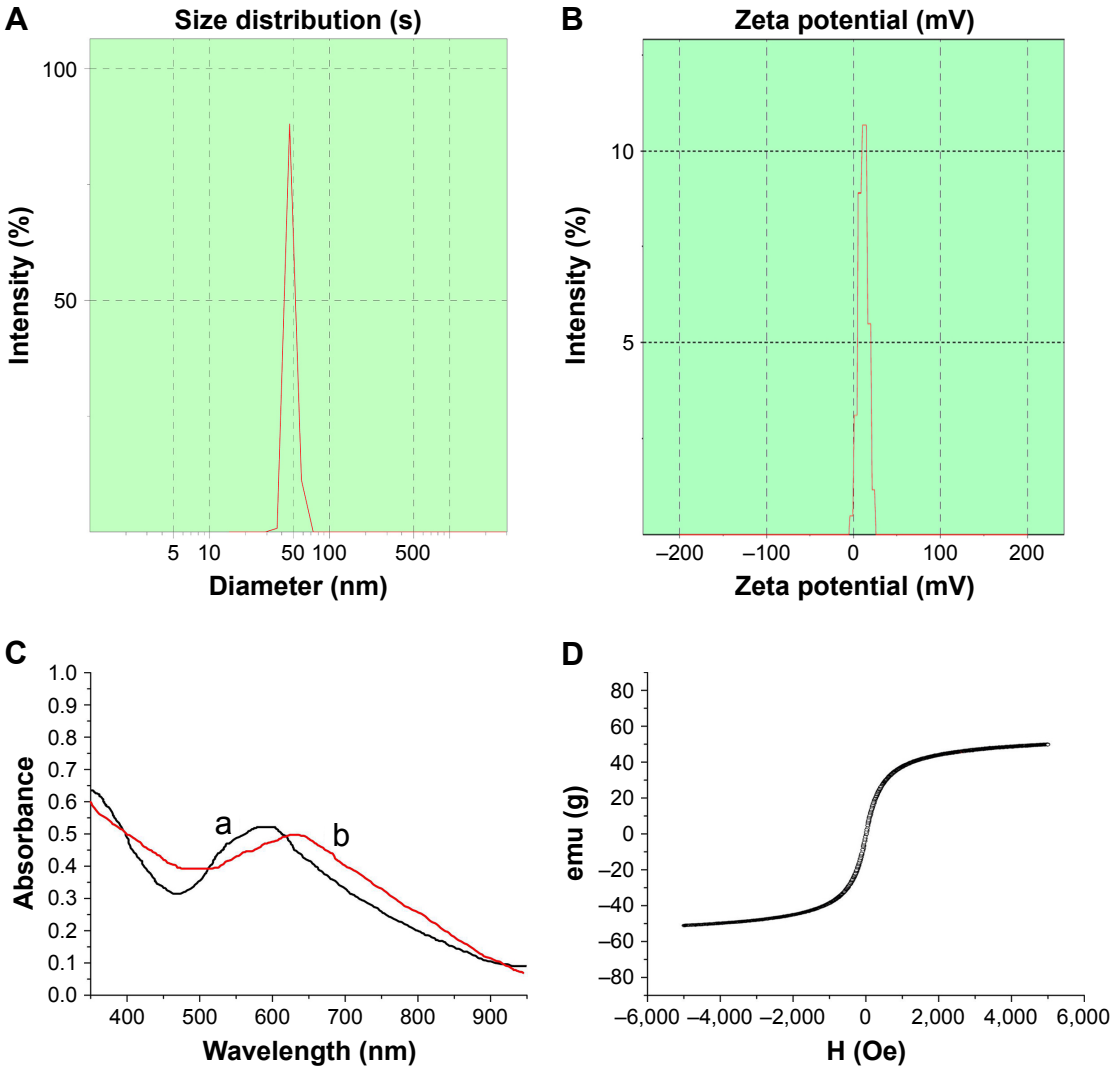

Figure 2 Characterization of Fe_3O_4@Au-C225 MNPs.
Notes: (**A**) Hydrodynamic diameter distribution of Fe_3O_4@Au-C225 MNPs; (**B**) Zeta potential of Fe_3O_4@Au-C225 MNPs; (**C**) UV–vis absorption spectra of Fe_3O_4@Au-C225 MNPs (curve b) and Fe_3O_4@Au MNPs (curve a). (**D**) The hysteresis loops of Fe_3O_4@Au-C225 MNPs.
Abbreviations: C225, cetuximab; MNPs, magnetic nanoparticles.

differences in the peak absorption wavelengths. Specifically, the absorption peak of Fe_3O_4@Au-C225 MNPs (630 nm) was red-shifted compared to that of Fe_3O_4@Au MNPs (612 nm; Figure 2C), which indicated excellent adsorption of C225.

Magnetic hysteresis measurements revealed that the magnetization of Fe_3O_4@Au-C225 MNPs shortly became saturated and exhibited zero remanence or coercive force, with the hysteresis loop close to the coincident "S"-shaped curve (Figure 2D). It provided a good demonstration of the superparamagnetic properties with Fe_3O_4@Au-C225 MNPs. The saturation magnetization value obtained from the hysteresis loops at 300 K is 51.2 emu/g Fe_3O_4@Au-C225 MNPs, which was close to Fe_3O_4@Au MNPs (51.8 emu/g).[32]

Determination of C225 adsorption

After being incubated with FITC-conjugated AffiniPure Goat Anti-Human IgG, green fluorescence from Fe_3O_4@Au-C225 MNPs was observed by confocal laser scanning microscope. In contrast, no fluorescence was detected in the Fe_3O_4@Au MNPs (Figure 3A and B).

Absorption efficiency

C225 absorption efficiency was determined by measuring the fluorescence percentage. The mean density and fluorescence percentage of Fe_3O_4@Au-C225 MNPs after incubation with FITC-conjugated AffiniPure Goat Anti-Human IgG were much higher than Fe_3O_4@Au-C225 MNPs without incubation with FITC-conjugated AffiniPure Goat Anti-Human IgG (Figure 4A and B), showing an effective antibody absorption.

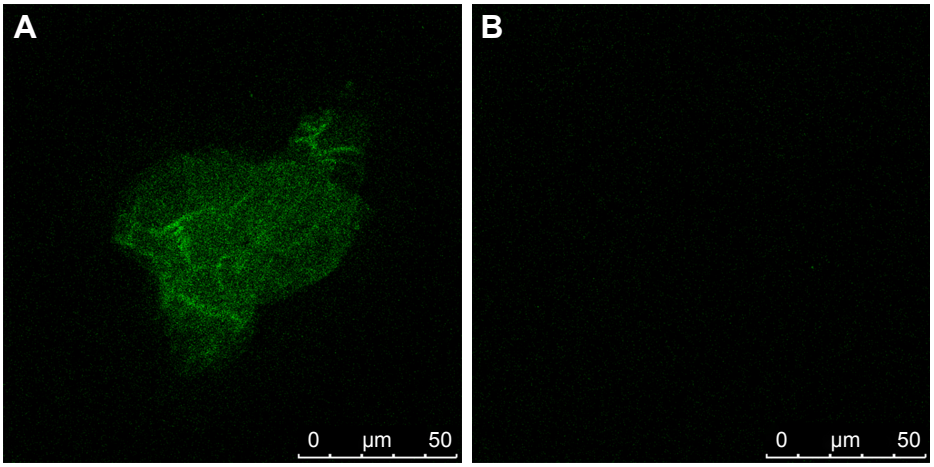

Figure 3 Determination of C225 absorbed on the surface of Fe_3O_4@Au-C225 MNPs.
Notes: (**A**) The green fluorescence was seen in the Fe_3O_4@Au-C225 MNPs; (**B**) No fluorescence could be detected in Fe_3O_4@Au MNPs.
Abbreviations: C225, cetuximab; MNPs, magnetic nanoparticles.

The binding of Goat Anti-Human IgG (Fc)-HRP at different dilutions to adsorbed Fe_3O_4@Au-C225 MNPs solution prepared was indicated by OD, and Fe_3O_4@Au-BSA and C225 mixture was used as control. To obtain the Fc binding efficiency of Fe_3O_4@Au MNPs toward C225, a percentage of Fe_3O_4@Au-C225 MNPs solution OD versus Fe_3O_4@Au-BSA and C225 mixture OD was calculated as shown in Table 1. It was found that the Fc binding of C225 was significant.

Heat generation by Fe_3O_4@Au-C225 MNPs in suspension

The iron concentrations of the Fe_3O_4@Au-C225 MNPs were ranging from 0.25 to 1.25 mg Fe/mL. When varying concentrations of Fe_3O_4@Au-C225 MNPs were exposed to AMF, the temperature rose rapidly within the first 30 min, then rose gently, and stabilized at a certain level after 50 min (Figure 5A). When exposed to NIR, the temperature rose rapidly within the first 15 min and stabilized at a certain level after 30 min (Figure 5B). When exposed to AMF+NIR, the temperature rose rapidly within the first 15 min and stabilized at a certain level after 20 min (Figure 5C). In three heating protocols, the rise in temperature increased with the iron concentration. Among all of the tested concentrations, 0.5 mg Fe/mL was the optimum. This hyperthermic behavior contributes to the killing of tumor cells while not harming normal tissues. In addition, Fe_3O_4@Au-C225 MNPs with the concentration of 0.5 mg Fe/mL exhibited a sufficient heating capacity (specific absorption rate [SAR]=84.56, intrinsic loss power [ILP]=0.018) to achieve satisfactory temperatures, which were selected in the following experiments. Temporal

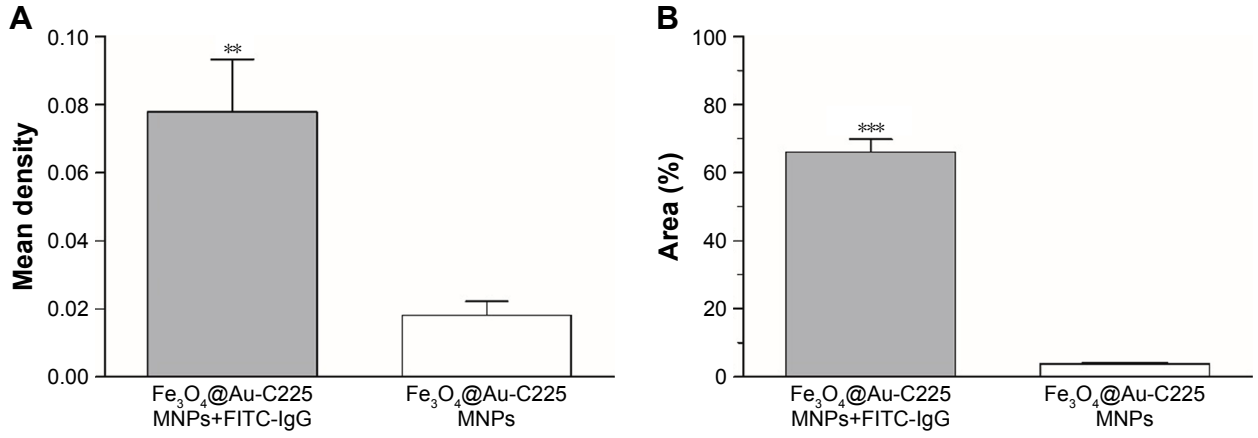

Figure 4 Determination of the C225 absorption efficiency by measuring mean density and fluorescence percentage.
Notes: (**A**) Mean density of Fe_3O_4@Au-C225 MNPs after incubation with FITC-labeled IgG and Fe_3O_4@Au-C225 MNPs without incubation with FITC-labeled IgG. (**B**) Fluorescence percentage of Fe_3O_4@Au-C225 MNPs after incubation with FITC-labeled IgG and Fe_3O_4@Au-C225 MNPs without incubation with FITC-labeled IgG. $^{**}P<0.01$; $^{***}P<0.001$.
Abbreviations: C225, cetuximab; FITC, fluorescein isothiocyanate; IgG, immunoglobulin G; MNPs, magnetic nanoparticles.

Table 1 Adsorption effect of Fe_3O_4@Au-C225 to antibody Fc

Dilution factor	Fe_3O_4@ Au-C225	Fe_3O_4@ Au-BSA, C225	Adsorption rate (%)
500	0.7820	0.8130	96.19
1,000	0.7360	0.7780	94.60
2,000	0.7340	0.7890	93.03
4,000	0.6060	0.6540	92.66
8,000	0.5340	0.5820	91.75
16,000	0.3460	0.3780	91.53

Abbreviations: BSA, bovine serum albumin; C225, cetuximab.

response curves for iron concentration of 0.5 mg Fe/mL in different heating protocols are also shown in Figure 5D.

Tumor cell proliferation and cellular apoptosis study in vitro

Fe_3O_4 MNPs, Fe_3O_4@Au MNPs, and Fe_3O_4@Au-C225 MNPs were incubated with U251 cells for 24 h. The cellular internalization of different nanoparticles was observed by reverse microscopy (Figure 6A).

MTT assay was performed to measure viability of U251 glioma cells after hyperthermia (nonhyperthermia or MFH alone or NIR alone or MFH+NIR) mediated by Fe_3O_4 MNPs, Fe_3O_4@Au MNPs, C225, Fe_3O_4@Au-C225 MNPs, and untreated cells as control. The cell RGR was calculated as (OD of experimental group/OD of blank control group)×100%.

When comparing the antiproliferation results (Figure 6B), it was found that the combined hyperthermia (MFH+NIR) mediated by Fe_3O_4@Au-C225 MNPs or Fe_3O_4@Au MNPs significantly decreased the cell viability ($P<0.05$), compared to sole hyperthermia (MFH or NIR). Moreover, significant loss in cell viability in U251 cells was observed after combined hyperthermia (MFH+NIR) mediated by Fe_3O_4@Au-C225 MNPs, and superior to that mediated by Fe_3O_4@

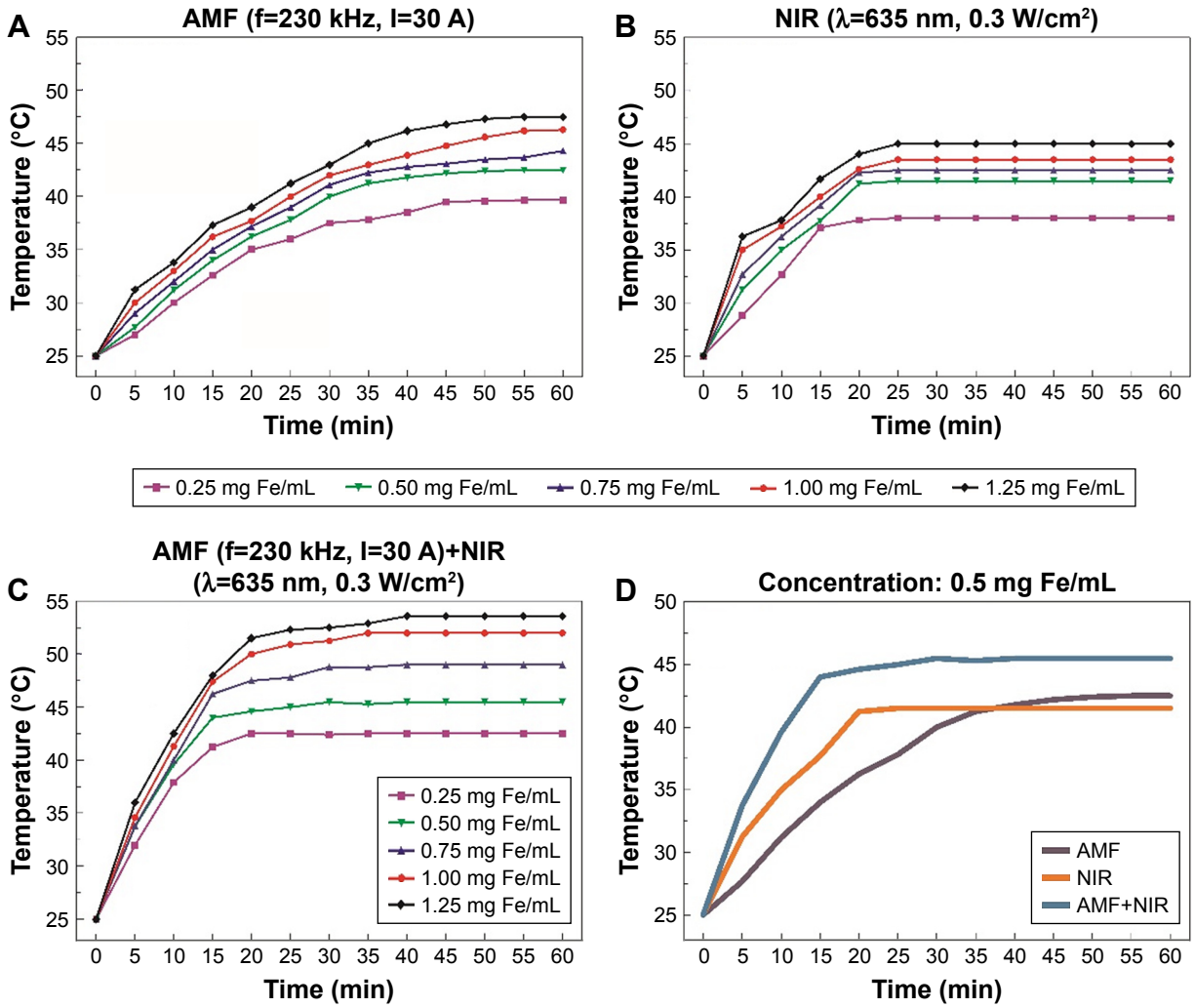

Figure 5 Heat generation by Fe_3O_4@Au-C225 MNPs in suspension (0.25–1.25 mg Fe/mL).
Notes: (**A**) AMF (f=230 kHz, I=30 A), (**B**) NIR (λ=635 nm, 0.3 W/cm²), and (**C**) AMF (f=230 kHz, I=30 A) combined with NIR (λ=635 nm, 0.3 W/cm²). (**D**) Temporal response curves for concentration of 0.5 mg Fe/mL.
Abbreviations: AMF, alternating magnetic field; MNPs, magnetic nanoparticles; C225, cetuximab; NIR, near-infrared hyperthermia.

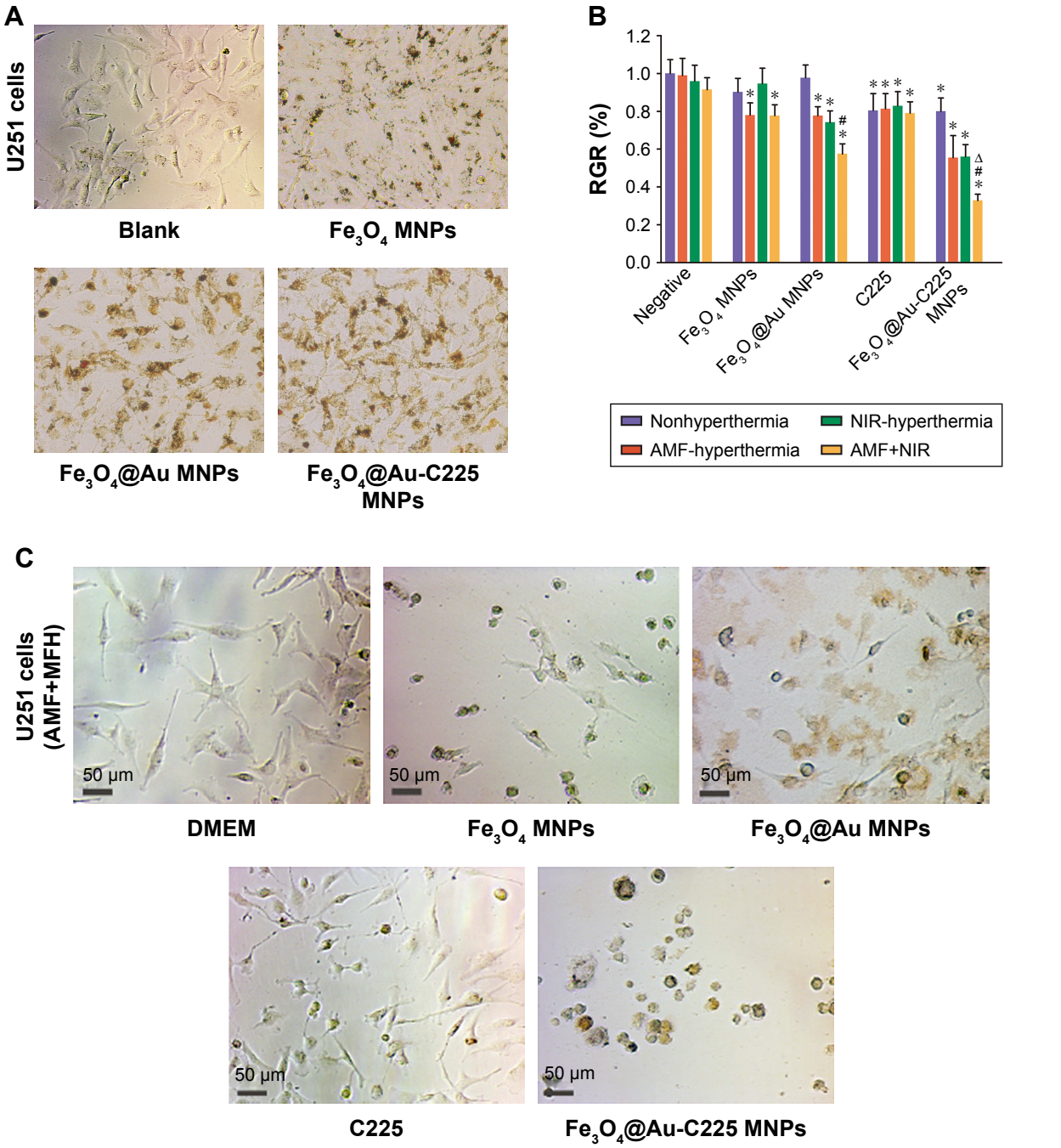

Figure 6 Proliferation of U251 cells after different treatments.

Notes: (**A**) Fe_3O_4 MNPs, Fe_3O_4@Au MNPs, and Fe_3O_4@Au-C225 MNPs were incubated with U251 cells. (**B**) The cell RGR of U251 glioma cells with different treatments ($\bar{x}\pm S$). (**C**) U251 cells were treated with combined hyperthermia (MFH+NIR) mediated by different nanoparticles. *Compared with the negative control group, $P<0.05$; #AMF+NIR group compared with AMF or NIR group, $P<0.05$; ΔFe_3O_4@Au-C225 MNPs compared with Fe_3O_4@Au MNPs when exposed to AMF combined with NIR, $P<0.05$.

Abbreviations: AMF, alternating magnetic field; C225, cetuximab; DMEM, Dulbecco's Modified Eagle's Medium; MFH, magnetic fluid hyperthermia; MNPs, magnetic nanoparticles; NIR, near-infrared hyperthermia; RGR, relative growth rate.

Au MNPs ($P<0.05$; Figure 6B and C), indicating the highest antiproliferative activity against U251 cells in this study.

For further investigation of the antiproliferative effect, the cell cycle progression was measured using flow cytometry. Results showed that S arrest was prominent in U251 cells exposed to Fe_3O_4@Au-C225 MNPs with or without hyperthermia (Figure 7). We also observed an increase in the percentage of apoptotic cells in Fe_3O_4@Au MNPs+MFH group (7.92%), Fe_3O_4@Au MNPs+NIR group (8.15%), Fe_3O_4@Au MNPs+MFH+NIR group (12.37%), Fe_3O_4@Au-C225 MNPs group (5.77%), Fe_3O_4@Au-C225 MNPs+MFH group (21.97%), Fe_3O_4@Au-C225 MNPs+NIR group (21.89%), and Fe_3O_4@Au-C225 MNPs+MFH+NIR group (46.21%), compared to negative control without a clear

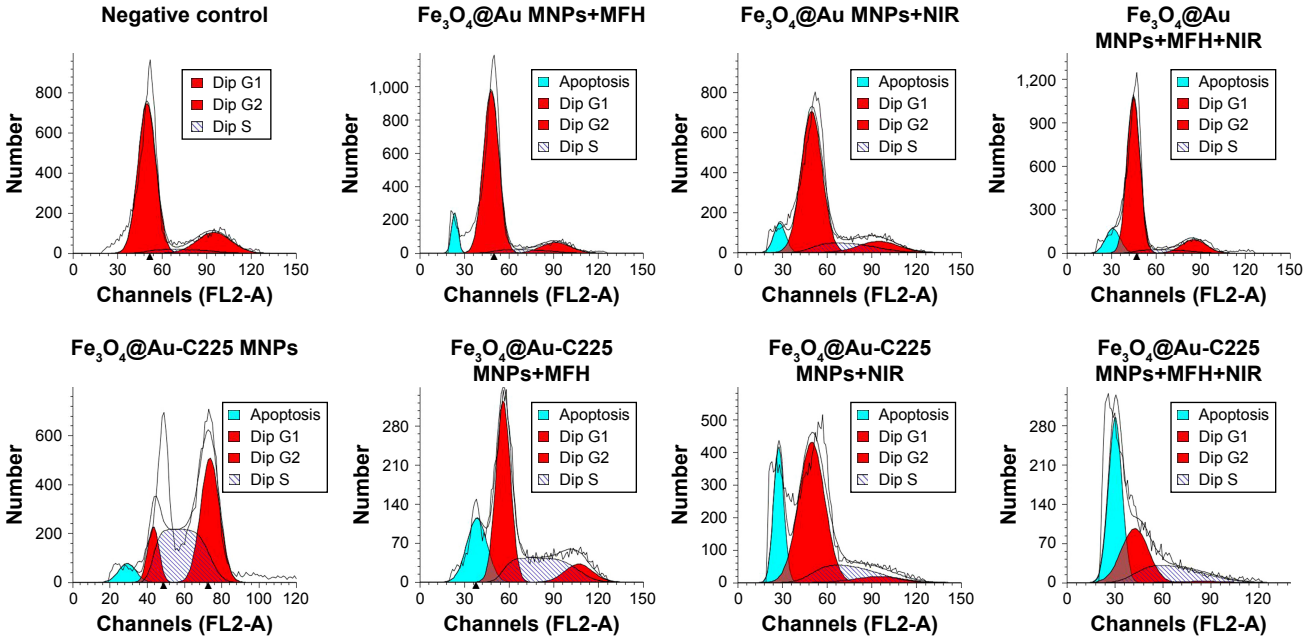

Figure 7 The flow cytometry analysis of U251 cells after different treatments.
Note: Apoptosis peak were observed in Fe_3O_4@Au MNPs+MFH group (7.92%), Fe_3O_4@Au MNPs+NIR group (8.15%), Fe_3O_4@Au MNPs+MFH+NIR group (12.37%), Fe_3O_4@Au-C225 MNPs group (5.77%), Fe_3O_4@Au-C225 MNPs+MFH group (21.97%), Fe_3O_4@Au-C225 MNPs+NIR group (21.89%), and Fe_3O_4@Au-C225 MNPs+MFH+NIR group (46.21%), comparing to negative control group without obvious apoptosis peak.
Abbreviations: C225, cetuximab; MFH, magnetic fluid hyperthermia; MNPs, magnetic nanoparticles; NIR, near-infrared hyperthermia.

hypodiploid peak. The highest hypodiploid peak indicated an excellent therapeutic efficacy of combined hyperthermia (MFH+NIR) mediated by Fe_3O_4@Au-C225 MNPs toward U251 cells by induction of apoptosis.

To evaluate the molecular mechanisms of Fe_3O_4@Au-C225 MNPs-mediated hyperthermia-induced apoptosis, we performed qRT-PCR and Western blot analyses. The results demonstrated that when compared to Fe_3O_4@Au MNPs-mediated hyperthermia, Fe_3O_4@Au-C225 MNPs-mediated hyperthermia successfully upregulated the mRNA and protein levels of caspase-3, caspase-8, and caspase-9 in U251 cells (Figure 8A–D). In addition, a marked upregulation of caspase-3, caspase-8, and caspase-9 expression, particularly caspase-3 and caspase-9, was evaluated using the cells treated with Fe_3O_4@Au-C225 MNPs-mediated combined hyperthermia (MFH+NIR), indicating the excellent antitumor effect of Fe_3O_4@Au-C225 MNPs-mediated combined hyperthermia by inducing intrinsic apoptosis in this study.

Study of Fe_3O_4@Au-C225 MNPs on human glioma U251 cells in vivo

A subcutaneous tumor model of U251 glioma cells was used to evaluate the in vivo therapeutic efficacy of Fe_3O_4@Au-C225 MNPs-mediated combined hyperthermia (MFH+NIR) in comparison with that mediated by Fe_3O_4@Au MNPs. At 42 days post-treatment, mice in groups were killed and the stripped tumor volume and weight were measured (Figure 9A and B). Compared to the negative control, the tumor growth was suppressed to various degrees in the tumor weight and volume among experimental groups ($P<0.05$; Figure 9A, left and right). Furthermore, treatments with Fe_3O_4@Au-C225 MNPs-mediated combined hyperthermia had more efficiency in reduction of tumor growth than that of the Fe_3O_4@Au MNPs-mediated combined hyperthermia ($P<0.05$; Figure 9A, left and right).

Subsequently, we performed histologic examinations of tumor tissues post-treatment via hematoxylin/eosin staining (Figure 9C). The tumor cells grew densely in the groups of control, Fe_3O_4@Au MNPs+MFH, Fe_3O_4@Au MNPs+NIR, and Fe_3O_4@Au-C225 MNPs. In the Fe_3O_4@Au MNPs+MFH+NIR, Fe_3O_4@Au-C225 MNPs+MFH, Fe_3O_4@Au-C225 MNPs+NIR, and Fe_3O_4@Au-C225 MNPs+MFH+NIR groups, the tumor cells atrophied and obvious zones of necrosis were observed in Fe_3O_4@Au-C225 MNPs+MFH+NIR group.

Ultrastructural characteristics of the tumor in Fe_3O_4@Au-C225 MNPs+MFH+NIR group were observed. TEM revealed intracellular localization of Fe_3O_4@Au-C225 MNPs. Numerous vesicles containing the aggregative Fe_3O_4@Au-C225 MNPs were visible intracellularly and were dispersed randomly in the cytoplasm (Figure 9D).

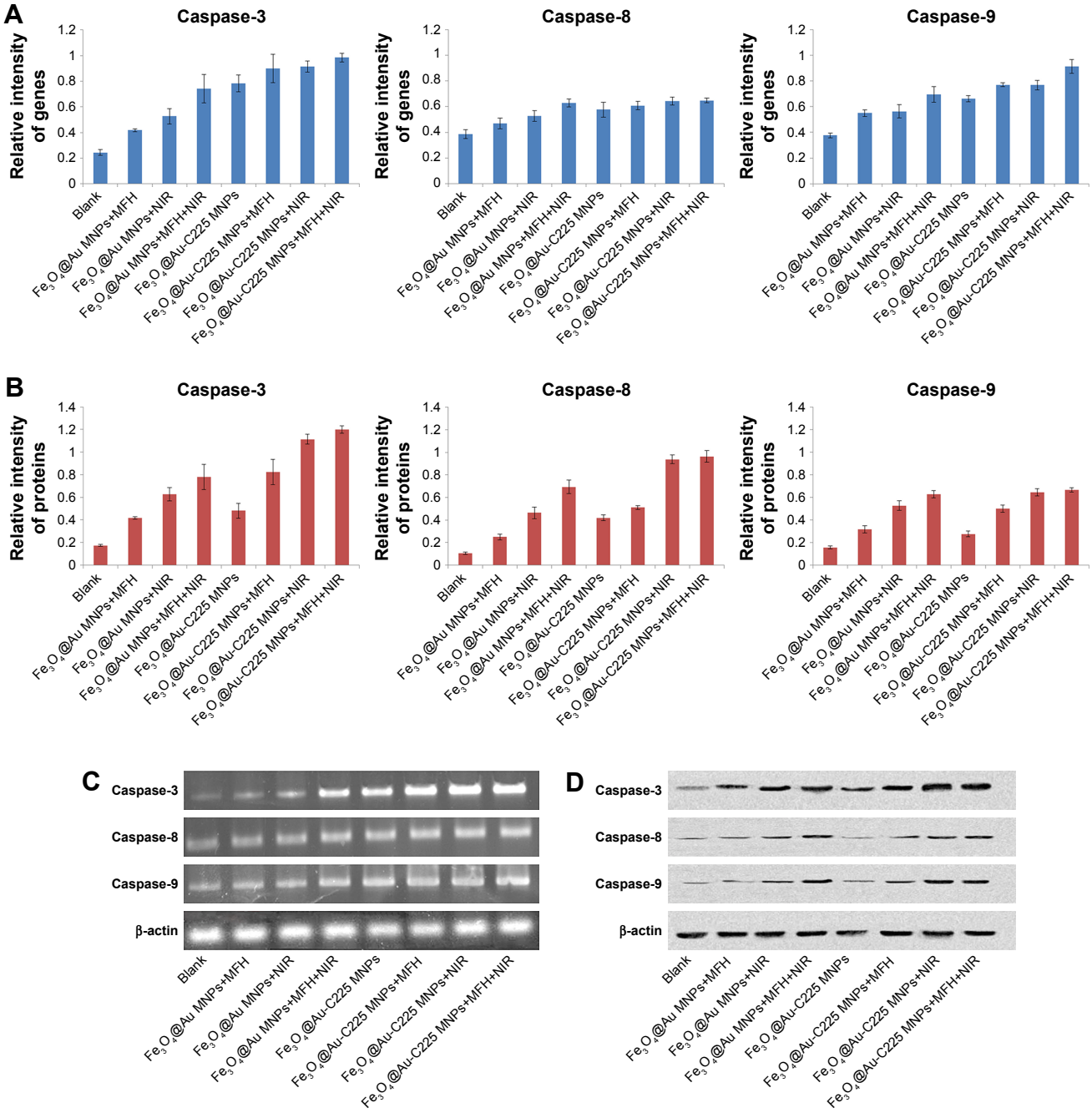

Figure 8 qRT-PCR and Western blot analyses of U251 cells after different treatments.
Notes: (**A**) The quantitative real-time polymerase chain reaction analyses to evaluate the relative mRNA levels of caspase-3, caspase-8, and caspase-9 in U251 cells with various treatments and (**C**) β-actin was used as an internal control to normalize the data. (**B**) Western blot analyses to evaluate the protein levels of caspase-3, caspase-8, and caspase-9 in U251 cells of different treatment groups, and (**D**) β-actin was used as an internal control to normalize the data.
Abbreviations: MFH, magnetic fluid hyperthermia; MNPs, magnetic nanoparticles; NIR, near-infrared hyperthermia.

Scattered and chaotic collagen fibers (Figure 9E) were also shown on the TEM micrographs.

Discussion

The combination of chemotherapy and thermotherapy has been the focus of cancer therapy in recent years. However, one of the challenges encountered was to achieve the optimal effects of the combination therapy. Thus, a robust therapeutic platform is urgently needed to achieve the most effective synergic effect for tumor therapy.

The importance of EGFR in the malignant progression of glioblastoma and the effect of EGFR on patient survival has been extensively documented. Overexpressed EGFR is present in up to 40% of primary glioblastoma and the

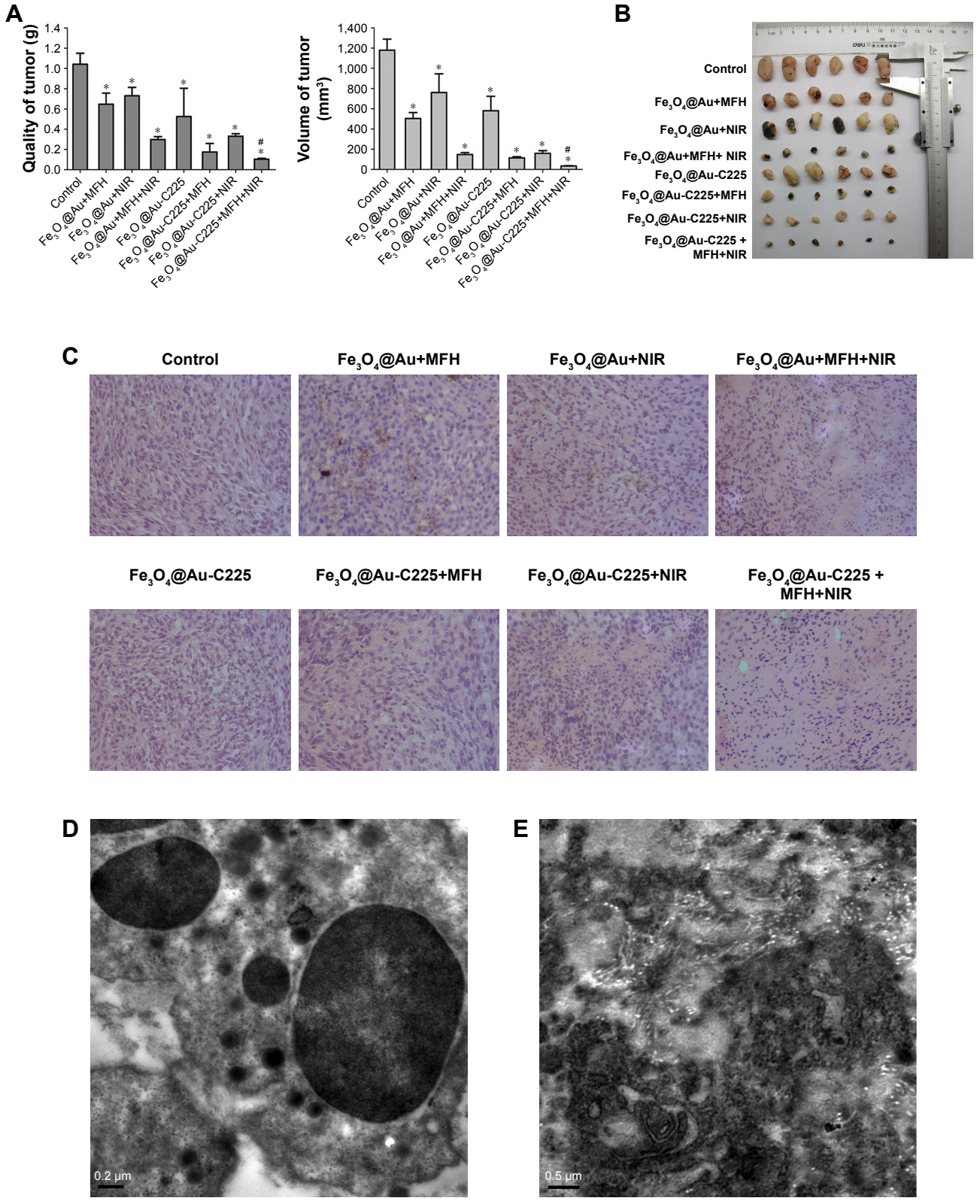

Figure 9 Efficacy of various therapeutic strategies in treating nude mice bearing U251 glioma tumors.

Notes: (**A**) The quality and volume changes of stripped tumors in various treatment groups. (**B**) Tumors rejected from mice in various treatment groups. (**C**) Histopathologic examination of human glioma transplanted in nude mice (hematoxylin/eosin staining, ×100 magnification). Transmission electron microscopy of the tumors exposed to Fe_3O_4@Au-C225 MNPs-mediated combined hyperthermia (MFH+NIR). (**D**) Numerous vesicles containing the aggregative Fe_3O_4@Au-C225 MNPs. (**E**) The denatured collagen zones in the close vicinity of Fe_3O_4@Au-C225 MNPs localization. *Compared with the negative control group, $P<0.05$; #Fe_3O_4@Au-C225 MNPs compared with Fe_3O_4@Au MNPs when exposed to AMF combined with NIR, $P<0.05$.

Abbreviations: AMF, alternating magnetic field; C225, cetuximab; MFH, magnetic fluid hyperthermia; MNPs, magnetic nanoparticles; NIR, near-infrared hyperthermia.

common overexpression makes EGFR a theoretically attractive target, and consequently, EGFR inhibitors have been among the most studied in clinical trials.[35–38] C225, an IgG1 human–murine chimeric of McAb M225 from murine, has been approved for use in patients with head and neck cancer, which is the only EGFR inhibitor that has conferred a survival advantage when combined with platinum-based combination chemotherapy.[39]

In this study, we decorated Fe_3O_4@Au composite MNPs with C225 via physical adsorption in order to maintain the biologic activities of C225. The green fluorescence observed by confocal laser scanning microscope (Figure 3A and B) and the UV–vis absorption spectra of Fe_3O_4@Au-C225 MNPs demonstrated the presence of C225 on the surface of Fe_3O_4@Au-C225 MNPs. The absorption peak of Fe_3O_4@Au-C225 MNPs (630 nm) was red-shifted compared to Fe_3O_4@Au MNPs (612 nm; Figure 2C), suggesting the excellent adsorption of C225. In addition, zeta potential and particle size are two important factors. The size of the nanoparticle may have an effect on uptake efficiency. The Fe_3O_4@Au-C225 MNPs that we synthesized revealed a diameter of 46 nm with a zeta potential of 11.1±1.8 mV. It is known that a nanoparticle with a positive charge has more efficient cellular internalization than a nanoparticle with a neutral or negative charge.[40,41] Cell surface usually has a negative charge; therefore, Fe_3O_4@Au MNPs (zeta potential=–23.2±1.8 mV) have less affinity to cancer cells because of negatively charged Au shell on its surface. Hence, C225 adsorption changed the zeta potential of the Fe_3O_4@Au-C225 MNPs to a positive charge, which possibly enhances the interaction between the nanoparticles and glioma cells. Perhaps more importantly, Fe_3O_4@Au-C225 MNPs may enter glioma cells through receptor-dependent C225-mediated endocytosis.

In our cell studies, MTT assay showed that the combined hyperthermia (MFH+NIR) mediated by Fe_3O_4@Au-C225 MNPs significantly decreased the U251 cell viability compared to sole hyperthermia (MFH or NIR), suggesting the optimizing heating efficiency. In addition, the highly antiproliferative effect of combined hyperthermia (MFH+NIR) mediated by Fe_3O_4@Au-C225 MNPs against U251 cells was also observed compared to that mediated by Fe_3O_4@Au MNPs groups, confirming the significant role of C225 in the targeting to U251 cells with overexpressed EGFR. For further investigation of the antiglioma effect, the cell cycle progression was measured using flow cytometry, and then qRT-PCR and Western blot analyses were performed to evaluate the molecular mechanisms of induced apoptosis. The combined hyperthermia (MFH+NIR) mediated by Fe_3O_4@Au-C225 MNPs exhibited excellent therapeutic efficacy for U251 cells by induction of apoptosis (Figure 7). Furthermore, a marked upregulation of caspase-3, caspase-8, and caspase-9 expression, particularly caspase-3 and caspase-9, was evaluated using the cells treated with Fe_3O_4@Au-C225 MNPs-mediated combined hyperthermia (MFH+NIR), indicating its excellent antitumor effect by inducing intrinsic apoptosis (Figure 8).

Evaluation of animal models displayed that therapeutic efficacy of Fe_3O_4@Au-C225 MNPs-mediated combined hyperthermia (MFH+NIR) was superior compared to sole hyperthermia (MFH or NIR) and Fe_3O_4@Au MNPs-mediated combined hyperthermia in mice with tumor model of human glioma. Representative sections of tumors are shown in Figure 9C. Control tumors, as well as NIR or MFH-treated tumors, exhibited a relatively viable and homogenous tumor tissue. The Fe_3O_4@Au-C225 MNPs did not affect the viability of U251 cells when hyperthermia was not applied, as neither zones of necrosis nor immune cell infiltrates were observed. In contrast, combined hyperthermia led to diffusion and subsequent dilution of Fe_3O_4@Au-C225 MNPs throughout the tumors, and enlarging zones of necrosis were also observed. TEM revealed intracellular localization of Fe_3O_4@Au-C225 MNPs. Numerous vesicles containing the aggregative Fe_3O_4@Au-C225 MNPs were visible intracellularly and were dispersed randomly in the cytoplasm (Figure 9D). The denatured collagen zones in the close vicinity of Fe_3O_4@Au-C225 MNPs localization were shown on the TEM micrographs (Figure 9E).

Structural modification of nanoparticles with targeting ligands like aptamers, short peptides, and other small molecules has been found to increase the accumulation of nanoparticles at the tumor site just because the ligands can recognize special and unique biophysical markers on the surface of tumor cells.[42–44] Therefore, in our study, designed Fe_3O_4@Au-C225 composite-targeted MNPs with C225, with high affinity for EGFR, caused to enhanced efficacy of cellular MNPs uptake through receptor-dependent C225-mediated endocytosis and antiglioma effect of C225 itself. Subsequently, the simultaneous application of both MFH and NIR hyperthermia contributes to intrinsic apoptosis of U251 glioma cells and enhanced efficacy in tumor size reduction. We developed a robust therapeutic platform for glioma therapy based on Fe_3O_4@Au-C225 composite-targeted MNPs. On the basis of the experimental results of this study, MFH combined with NIR hyperthermia mediated by Fe_3O_4@Au-C225 composite-targeted MNPs will show promise in future human clinical trial for patients with glioma.

Conclusion

We developed a robust therapeutic platform for tumor therapy based on Fe_3O_4@Au-C225 composite-targeted MNPs. C225 was physically adsorbed to the surface of Fe_3O_4@Au MNPs. Furthermore, the dual magnetic and photothermal action mediated by Fe_3O_4@Au-C225 composite-targeted MNPs resulted in intrinsic apoptosis of U251 cells in vitro and growth suppression of tumor in vivo, which showed remarkable improvement in synergistic therapeutic effects for glioma treatment.

Acknowledgments

This work was supported by the National Natural Science Foundation of China (grant number: 81301313; 81600159), the Natural Science Foundation of Jiangsu Province (grant number: BK20131015; BK20141015), Jiangsu Provincial College Students' Practical Innovation Training Program (grant number: 201410312015Z), and Nanjing Developing Project of Medical Science (grant number: YKK13174).

Disclosure

The authors declare no conflicts of interest in this work.

References

1. Anjum K, Shagufta BI, Abbas SQ, et al. Current status and future therapeutic perspectives of glioblastoma multiforme (GBM) therapy: a review. *Biomed Pharmacother*. 2017;92:681–689.
2. Parasramka S, Talari G, Rosenfeld M, Guo J, Villano JL. Procarbazine, lomustine and vincristine for recurrent high-grade glioma. *Cochrane Database Syst Rev*. 2017;7(1):CD011773.
3. Ferlay J, Soerjomataram I, Dikshit R, et al. Cancer incidence and mortality worldwide: sources, methods and major patterns in GLOBOCAN 2012. *Int J Cancer*. 2015;136(5):E359–E386.
4. *Cancer Facts & Figures 2017*. Atlanta, GA: American Cancer Society; 2017.
5. Brandes AA, Tosoni A, Franceschi E, Reni M, Gatta G, Vecht C. Glioblastoma in adults. *Crit Rev Oncol Hematol*. 2008;67(2):139–152.
6. Glaser T, Han I, Wu L, Zeng X. Targeted nanotechnology in glioblastoma multiforme. *Front Pharmacol*. 2017;8:166.
7. Tosi U, Marnell CS, Chang R, et al. Advances in molecular imaging of locally delivered targeted therapeutics for central nervous system tumors. *In J Mol Sci*. 2017;18(2):E351.
8. Reni M, Mazza E, Zanon S, Gatta G, Vecht CJ. Central nervous system gliomas. *Crit Rev Oncol Hematol*. 2017;113:213–234.
9. Seystahl K, Papachristodoulou A, Burghardt I, et al. Biological role and therapeutic targeting of TGF-β3 in glioblastoma. *Mol Cancer Ther*. 2017;16(6):1177–1186.
10. Zhou J, Tien AC, Alberta JA, et al. A sequentially priming phosphorylation cascade activates the gliomagenic transcription factor olig2. *Cell Rep*. 2017;18(13):3167–3177.
11. Li Y, Lin T, Luo Y, et al. A smart and versatile theranostic nanomedicine platform based on nanoporphyrin. *Nat Commun*. 2014;5:4712.
12. Di Corato R, Béalle G, Kolosnjaj-Tabi J, et al. Combining magnetic hyperthermia and photodynamic therapy for tumor ablation with photoresponsive magnetic liposomes. *ACS Nano*. 2015;9(3):2904–2916.
13. Pasparakis G, Manouras T, Vamvakaki M, Argitis P. Harnessing photochemical internalization with dual degradable nanoparticles for combinatorial photo-chemotherapy. *Nat Commun*. 2014;5:3623.
14. Mu X, Zhang F, Kong C, et al. EGFR-targeted delivery of DOX-loaded Fe3O4@ polydopamine multifunctional nanocomposites for MRI and antitumor chemo-photothermal therapy. *Int J Nanomedicine*. 2017;12:2899–2911.
15. Lian HY, Hu M, Liu CH, Yamauchi Y, Wu KCW. Highly biocompatible, hollow coordination polymer nanoparticles as cisplatin carriers for efficient intracellular drug delivery. *Chem Commun (Camb)*. 2012;48(42):5151–5153.
16. Shieh FK, Wang SC, Yen CL, et al. Imparting functionality to biocatalysts via embedding enzymes into nanoporous materials by a de novo approach: size-selective sheltering of catalase in metal−organic framework microcrystals. *J Am Chem Soc*. 2015;137(13):4276–4279.
17. Liang YH, Liu CH, Liao SH, et al. Cosynthesis of cargo-loaded hydroxyapatite/alginate core-shell nanoparticles (HAP@Alg) as pH-responsive nanovehicles by a pre-gel method. *ACS Appl Mater Interfaces*. 2012;4(12):6720–6727.
18. Bastakoti BP, Hsu YC, Liao SH, et al. Inorganic-organic hybrid nanoparticles with biocompatible calcium phosphate thin shells for fluorescence enhancement. *Chem Asian J*. 2013;8(6):1301–1305.
19. Mcnamara K, Tofail SA. Nanosystems: the use of nanoalloys, metallic, bimetallic, and magnetic nanoparticles in biomedical applications. *Phys Chem Chem Phys*. 2015;17(42):27981–27995.
20. Tassa C, Shaw SY, Weissleder R. Dextran-coated iron oxide nanoparticles: a versatile platform for targeted molecular imaging, molecular diagnostics, and therapy. *Acc Chem Res*. 2011;44(10):842–852.
21. Lutz JF, Stiller S, Hoth A, Kaufner L, Pison U, Cartier R. One-pot synthesis of pegylated ultrasmall iron-oxide nanoparticles and their in vivo evaluation as magnetic resonance imaging contrast agents. *Biomacromolecules*. 2006;7(11):3132–3138.
22. Kohler N, Fryxell GE, Zhang M. A bifunctional poly(ethylene glycol) silane immobilized on metallic oxide-based nanoparticles for conjugation with cell targeting agents. *J Am Chem Soc*. 2004;126(23):7206–7211.
23. Masoudi A, Madaah Hosseini HR, Shokrgozar MA, Ahmadi R, Oghabian MA. The effect of poly(ethylene glycol) coating on colloidal stability of superparamagnetic iron oxide nanoparticles as potential MRI contrast agent. *Int J Pharm*. 2012;433(1–2):129–141.
24. Ma D, Guan J, Dénommée S, Enright G, Veres T, Simard B. Multifunctional nano-architecture for biomedical applications. *Chem Mater*. 2006;18(7):1920–1927.
25. Ban Z, Barnakov YA, Li F, Goluba VO, O'Conno CJ. The synthesis of core–shell iron@gold nanoparticles and their characterization. *J Mater Chem*. 2005;15(43):4660–4662.
26. Chen M, Yamamuro S, Farrell D, Majetich SA. Gold-coated iron nanoparticles for biomedical applications. *J Appl Phys*. 2003;93(10):7551–7553.
27. Zhou T, Wu B, Xing D. Bio-modified Fe3O4 core/Au shell nanoparticles for targeting and multimodal imaging of cancer cells. *J Mater Chem*. 2011;22(2):470–477.
28. Brullot W, Valev VK, Verbiest T. Magnetic-plasmonic nanoparticles for the life sciences: calculated optical properties of hybrid structures. *Nanomedicine*. 2012;8(5):559–568.
29. Zhou H, Choi SI, Zou F, et al. Cytotoxicity and gene expression in sarcoma 180 cells in response to spiky magnetoplasmonic supraparticles. *ACS Appl Mater Interfaces*. 2014;6(22):19680–19689.
30. Zhou H, Zou F, Koh K, Lee J. Multifunctional magnetoplasmonic nanomaterials and their biomedical applications. *J Biomed Nanotechnol*. 2014;10(10):2921–2949.
31. Espinosa A, Di CR, Kolosnjaj-Tabi J, Flaud P, Pellegrino T, Wilhelm C. Duality of iron oxide nanoparticles in cancer therapy: amplification of heating efficiency by magnetic hyperthermia and photothermal bimodal treatment. *ACS Nano*. 2016;10(2):2436–2446.
32. Yuntao Li, Jing Liu, Yuejiao Zhong, et al. Biocompatibility of Fe3O4@Au composite magnetic nanoparticles in vitro and in vivo. *Int J Nanomedicine*. 2011;6:2805–2819.
33. Du Y, Zhang D, Liu H, Lai R. Thermochemotherapy effect of nanosized As2O3/Fe3O4 complex on experimental mouse tumors and its influence on the expression of CD44v6, VEGF-C and MMP-9. *BMC Biotechnol*. 2009;9:84.

34. Tzoneva R, Faucheux N, Groth T. Wettability of substrata controls cell-substrate and cell-cell adhesions. *Biochim Biophys Acta*. 2007;1770(11):1538–1547.
35. Wong AJ, Bigner SH, Bigner DD, Kinzler KW, Hamilton SR, Vogelstein B. Increased expression of the epidermal growth factor receptor gene in malignant gliomas is invariably associated with gene amplification. *Proc Natl Acad Sci U S A*. 1987;84(19):6899–6903.
36. van den Bent MJ, Brandes AA, Rampling R, et al. Randomized phase II trial of erlotinib versus temozolomide or carmustine in recurrent glioblastoma: EORTC brain tumor group study 26034. *J Clin Oncol*. 2009;27(8):1268–1274.
37. Lassman AB, Rossi MR, Raizer JJ, et al. Molecular study of malignant gliomas treated with epidermal growth factor receptor inhibitors: tissue analysis from North American Brain Tumor Consortium Trials 01-03 and 00-01. *Clin Cancer Res*. 2005;11(21):7841–7850.
38. Dokala A, Thakur SS. Extracellular region of epidermal growth factor receptor: a potential target for anti-EGFR drug discovery. *Oncogene*. 2017;36(17):2337–2344.
39. Herbst RS, Langer CJ. Epidermal growth factor receptors as a target for cancer treatment: the emerging role of IMC-C225 in the treatment of lung and head and neck cancers. *Semin Oncol*. 2002;29(29):27–36.
40. Chen X, Zhu X, Li L, et al. Investigation on novel chitosan nanoparticle-aptamer complexes targeting TGF-β receptor II. *Int J Pharm*. 2013;456(2):499–507.
41. Jo DH, Kim JH, Lee TG, Kim JH. Size, surface charge, and shape determine therapeutic effects of nanoparticles on brain and retinal diseases. *Nanomedicine*. 2015;11(7):1603–1611.
42. Wang H, Zhao X, Guo C, et al. Aptamer-dendrimer bioconjugates for targeted delivery of miR-34a expressing plasmid and antitumor effects in non-small cell lung cancer cells. *PLoS One*. 2015;10(9):e0139136.
43. Guo J, Gao X, Su L, et al. Aptamer-functionalized PEG–PLGA nanoparticles for enhanced anti-glioma drug delivery. *Biomaterials*. 2011;32(31):8010–8020.
44. Taghavi S, Nia AH, Abnous K, Ramezani M. Polyethylenimine-functionalized carbon nanotubes tagged with AS1411 aptamer for combination gene and drug delivery into human gastric cancer cells. *Int J Pharm*. 2017;516(1–2):301–312.